2011

Phr1 is required for proper retinocollicular targeting of nasal-dorsal retinal ganglion cells

Bradley Q. Vo
Washington University School of Medicine in St. Louis
A J. Bloom
Washington University School of Medicine in St. Louis
Susan M. Culican
Washington University School of Medicine in St. Louis

Visual Neuroscience (2011), **28**, 175–181.

doi:10.1017/S0952523810000386

BRIEF COMMUNICATION

Phr1 is required for proper retinocollicular targeting of nasal–dorsal retinal ganglion cells

BRADLY Q. VO,[1] A. JOSEPH BLOOM,[2] AND SUSAN M. CULICAN[1]

[1]Department of Ophthalmology and Visual Sciences, Washington University School of Medicine, Saint Louis, Missouri
[2]Department of Psychiatry, Washington University School of Medicine, Saint Louis, Missouri

(Received April 21, 2010; Accepted October 19, 2010; First Published Online February 16, 2011)

Abstract

Precise targeting of retinal projections is required for the normal development of topographic maps in the mammalian primary visual system. During development, retinal axons project to and occupy topographically appropriate positions in the dorsal lateral geniculate nucleus (dLGN) and superior colliculus (SC). *Phr1* retinal mutant mice, which display mislocalization of the ipsilateral retinogeniculate projection independent of activity and ephrin-A signaling, were found to have a more global disruption of topographic specificity of retinofugal inputs. The retinocollicular projection lacks local refinement of terminal zones and multiple ectopic termination zones originate from the dorsal–nasal (DN) retinal quadrant. Similarly, in the dLGN, the inputs originating from the contralateral DN retina are poorly refined in the *Phr1* mutant. These results show that *Phr1* is an essential regulator of retinal ganglion cell projection during both dLGN and SC topographic map development.

Keywords: dLGN, Superior colliculus, Retinocollicular, Topography, DiI

Introduction

Precise topographic mapping of retinal projections to central targets is a requisite of normal mammalian visual system development. The axons of neighboring retinal ganglion cells (RGCs) project to adjacent regions within the dorsal lateral geniculate nucleus (dLGN) and superior colliculus (SC) (reviewed in Reese, 2010). Topographic specificity is guided predominantly by reciprocal molecular gradients (Sperry, 1963) and refined in an activity-dependent fashion (Torborg & Feller, 2005). The Eph family receptor tyrosine kinases and their ligands, the ephrins, are the most thoroughly characterized molecular mediators of topographic specification (McLaughlin & O'Leary, 2005). EphAs and ephrin-As direct the mapping of RGC axons along the anterior–posterior axis of the SC according to the position of their cell bodies on the nasotemporal axis of the retina, whereas EphBs and ephrin-Bs direct mapping along the mediolateral axis of the SC according to their retinal dorsoventral position (Hindges et al., 2002; Luo & Flanagan, 2007). Ephrin signaling has also been shown necessary for topographic specificity in the dLGN (Pfeiffenberger et al., 2006), but the mechanisms of this patterning are less well understood, partly due to the three-dimensional structure of the nucleus.

Phr1 is an evolutionary conserved multidomain protein that plays a central role in neural development. Disruption of *Phr1* orthologs is associated with defects ranging from excess synaptic growth in Drosophila (Wan et al., 2000; DiAntonio et al., 2001), synaptogenesis, and axon termination defects in *Caenorhabditis elegans* (Schaefer et al., 2000; Zhen et al., 2000); abnormal retinal projections in zebrafish (D'Souza et al., 2005); and axon guidance defects in vertebrates (Burgess et al., 2004; Bloom et al., 2007). Complete knockout of *Phr1* is neonatally lethal in the mouse (Burgess et al., 2004; Bloom et al., 2007; Lewcock et al., 2007), and conditional knockout of *Phr1* in RGCs results in an abnormal localization of the ipsilateral retinogeniculate projection that is independent of ephrin-A responsiveness and spontaneous retinal activity (Culican et al., 2009). Here, we report a quadrant-specific disruption of the retinotopic map in the SC, with more subtle defects in the dLGN, indicating that *Phr1* is required to establish regional as well as global topography.

Materials and methods

Mice

Phr1 retinal mutant mice were described previously (Culican et al., 2009). Studies here were done in mice backcrossed into C57BL/6J background. Genotyping was done by PCR. Briefly, *Phr1* conditional knockout mice containing a floxed allele of *Phr1* were mated to mice that express Cre recombinase in RGCs under the control of the Math5 promoter (Yang et al., 2003).

RGC labeling

RGC labeling was adapted from Simon and O'Leary (1991). A 10% solution of the fluorescent lipophilic dye, 1, 1′-dioctadecyl-3,

Address correspondence and reprint requests to: Dr. Susan M. Culican, Department of Ophthalmology and Visual Sciences, Washington University School of Medicine, 660 South Euclid Avenue, Ophthalmology Box 8096, Saint Louis, MO 63110. E-mail: culican@vision.wustl.edu

3,3′,3′-tetramethylindocarbocyanine perchlorate (DiI; Invitrogen, Carlsbad, CA) in dimethylformamide (Sigma, St. Louis, MO), was pressure injected through a pulled glass micropipette using a Picospritzer II (General Valve Corp., Fairfield, NJ). Postnatal day 14 (P14) or older mice were anesthetized and injected with 0.1–1 μl of DiI in one eye through a small hole made in the sclera at the limbus with a 27 gauge needle. Injections were performed masked to genotype. Mice were sacrificed 6 days later (older then P20) and intercardially perfused with PBS then 4% paraformaldehyde in 0.1 M PBS. Brains were postfixed and whole-mount SCs imaged with a RoleraXR camera mounted on an Olympus BX51WI microscope (Olympus, Center Valley, PA). Brains were then embedded in 2–3% agarose (Sigma) and 100-μm coronal sections sliced on a Vibratome, mounted, and imaged. Image acquisition was performed masked to genotype.

Retrograde labeling

P14 mice were anesthetized and intercardially perfused with PBS then 4% paraformaldehyde in PBS. Brains were postfixed, and the cortex was removed. 0.1–0.5 μl of DiI was pressure injected as described above into the posterial–lateral region of the SC. After 14 days, whole-mount SC images were obtained. Brains were embedded in 2–3% agarose and 120-μm sagittal sections sliced and imaged.

Quantification and representation of data

Whole-mount SC image analysis was adapted from Pfeiffenberger et al. (2006). Images of whole-mount SC were opened in Image J (v.1.41; NIH Bethesda, MD) and background fluorescence levels, determined from measurement of a nonlabeled area of the SC, were digitally subtracted. An intensity plot of the contralateral SC was obtained covering a rectangular region one-third the lateral–medial (L-M) width of the SC and equal in length to the longest anterior-posterior (A-P) dimension. All intensity plots were normalized to an A-P length of 600 pixels.

Summary of ectopic termination zones in nasal–dorsal quadrant

Termination zones from four controls and four *Phr1* mutants were plotted along the anterior–posterior axis with 0 and 100 representing the posterior and anterior borders of the SC, respectively. Each point on the horizontal axis represents a single distinct termination zone along the anteroposterior extent of the nucleus, and each vertical set of points represents one animal after receiving a single retinal injection (adapted from Feldheim et al., 2000).

Quantification of area (in percentage) of terminal zones in SC and dLGN

The dLGN and SC were outlined manually based on gross anatomical morphology. Background fluorescence levels in the dLGN and SC were determined from measurement of a nonlabeled area of the dLGN and SC, respectively, and digitally subtracted. A threshold was set at 20% of the maximum signal intensity, and the area (in pixels) measured above that threshold was divided by the total area and reported as a percentage. For dLGN specifically, the total percentage for each animal was obtained by the averaging values from four slices (see Culican et al., 2009). Average area for each regional injection site was obtained by averaging the values from four animals in each condition. Errors are standard error mean. Composite panels were generated to qualitatively illustrate the extent of labeling in the dorsal–ventral and medial–lateral axis for each condition (Supplementary Fig. S1).

Results

Disrupted mapping along the nasal–dorsal axis of the Phr1 *mutant retinocollicular projection*

To evaluate retinocollicular connectivity in *Phr1* retinal mutants, we delivered focal DiI injections into the four retinal quadrants [nasal dorsal (ND), nasal ventral (NV), temporal dorsal (TD), and temporal ventral (TV)] and assessed axon termination in the SC. In control mice, a single injection resulted in a single compact terminal zone (TZ) on the outer edge of the SC corresponding to the peripheral injection site of each retinal quadrant (Fig. 1a–1d). ND and NV retinal injections produced compact TZs located in the posterior–lateral and posterior–medial regions of the SC, respectively (Fig. 1a and 1b). The location and continuity of the ipsilateral patch is disrupted in the dLGN of *Phr1* retinal mutant mice (Culican et al., 2009). Because RGC axons that project to the ipsilateral patch originate in the TV quadrant of the retina, we expected to also observe mislocalization of TZ in the SC from retinal axons of TV quadrant origin. But on the contrary, the most dramatic disruption was of DiI labeling from ND quadrant mutant RGCs. Labeling this quadrant lead to multiple ectopic TZs shifted anteromedially in the nucleus (Fig. 1a′ and 1e). Additionally, we observed a global disruption of local refinement of TZs in the *Phr1* retinal mutant; TZs derived from the ND, as well as from the other three quadrants, were more diffuse and occupied larger areas of the SC. The total area of the SC labeled after a single injection in retina mutants was significantly larger ($1.403 \pm 0.351\%$, $n = 16$) than in littermate controls ($0.976 \pm 0.244\%$, $n = 16$) ($P < 0.01$) (Fig. 1f). These results thus demonstrate that loss of *Phr1* in RGCs results in both a broad disruption of topographic connections along the ND retinal axis and a disruption of local TZ refinement along all retinal axes.

Ectopic termination zones do not result from interstitial branching

The cellular basis of ectopic TZs that arise from RGCs in the ND quadrant is unclear. One possibility is that nearest-neighbor relationships are not preserved in the *Phr1* retinal mutant and project to different locations within the SC. Another possibility is that nearest-neighbor relationships are preserved but that interstitial branching of RGC axonal arbors results in representations of the same retinotopic map in multiple locations. To assess whether the ectopic patches derived from the ND projection result from multiple representations of a properly organized retinotopic map, we employed retrograde DiI labeling. Focal DiI injections were made into the posterial–lateral region of the SC, the area where ND RGCs terminate. If the disrupted mapping of ND RGCs is due to multiple representations of the normal map caused by misdirected interstitial branching, then additional ectopic TZs anterior to the injection site should be observed (Fig. 2a–2b). In both control and mutant mice, injections of various sizes and locations within the posterial–lateral region do not yield additional termination zones (Fig. 2c–2n). Furthermore, observation of labeled primary axons traveling through the most anterior edges of the SC in these animals indicate that sufficient time was allowed for dye to travel (Fig. 2o–2p). These results suggest that the disrupted mapping along the ND axis of the *Phr1* mutant retinal projection is not caused by erroneous interstitial branching.

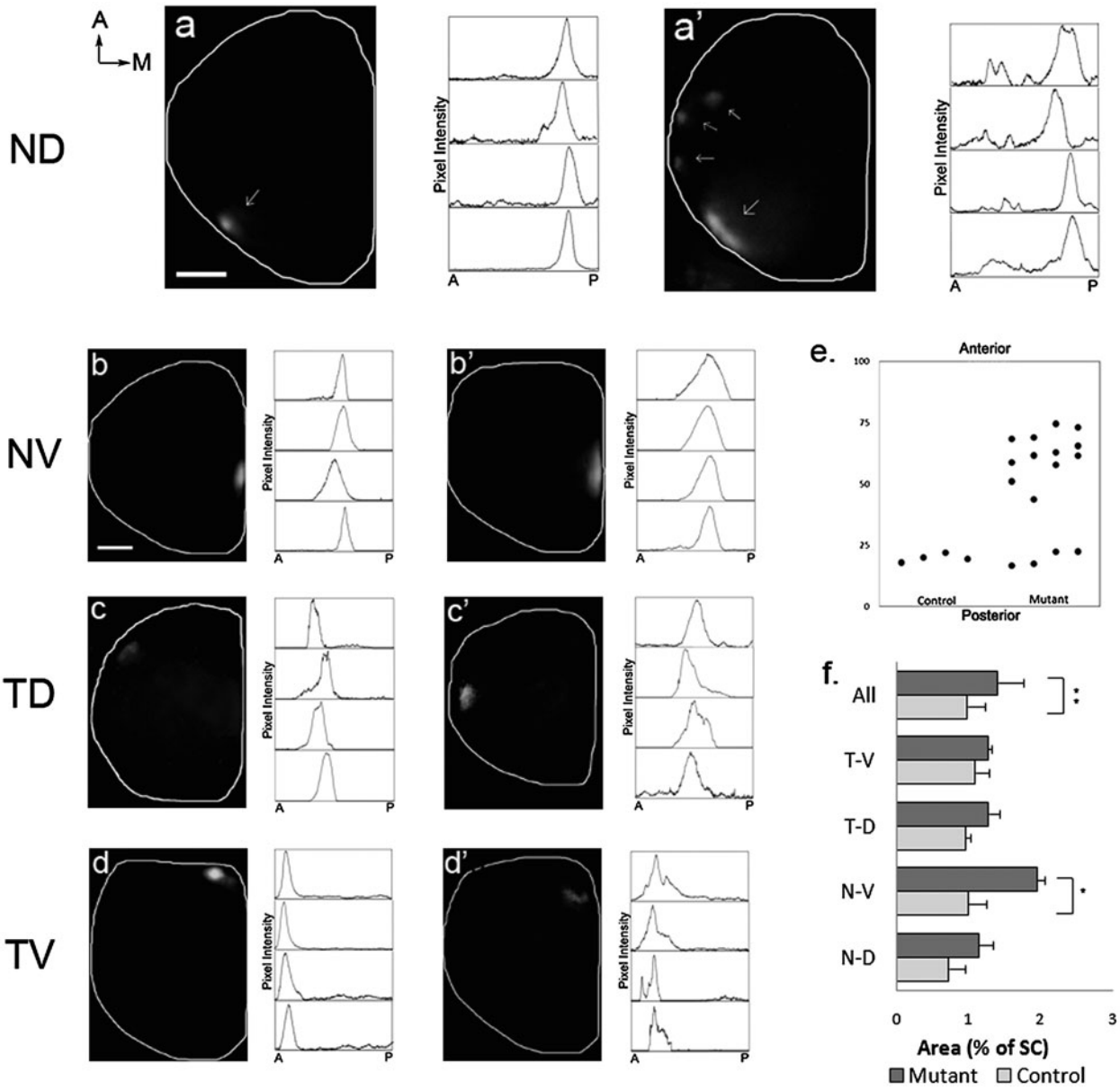

Fig. 1. *Phr1* retina mutants have multiple ectopic terminal zones (TZs) originating from the nasal–dorsal (ND) retina and aberrant diffuse disruption other quadrants. Retinal projections to the superior colliculus (SC) were compared between control (a–d) and *Phr1* mutant (a′d′). Multiple ectopic TZs are observed in the SC of the retinal mutant (a′) compared to a single compact TZ in control (a) with DiI injection in the ND quadrant of the retina. A summary of the topographic mapping defects from cells originating in the ND quadrant (e). Nasal–ventral (NV) (b, b′), temporal–dorsal (TD) (c, c′), and temporal–ventral (TV) (d, d′) RGCs from the mutant display more diffuse TZs compared to littermate controls. Intensity spikes indicate TZs in each intensity plot to the right. Diffuse TZs occupy a larger area (% of SC) in all quadrants (f). Mutant RGCs originating in the NV retina occupy a significantly larger area of the SC compared to control ($P < 0.05$). Differences in the other quadrants are not significant (TD, $P \sim 0.06$; ND, $P \sim 0.10$; TV, $P \sim 0.20$). Error bars represent standard error mean (S.E.M.). Total $n = 32$, $n = 4$ for each genotype and each quadrant. Scale bar = 400 μm; a, anterior; p, posterior; m, medial; d, dorsal; n, nasal; v, ventral; t, temporal.

Diffuse mapping along all axes in the Phr1 *mutant retinogeniculate projection*

Abnormal localization of the ipsilateral retinogeniculate projection was previously demonstrated in *Phr1* retinal mutants despite normal spontaneous retinal activity and eye-specific input segregation in these animals (Culican et al., 2009). However, it remained undetermined whether the erroneous projection resulted from a global shifting of the broad retinogeniculate map or rather as an indirect consequence of disrupted nearest-neighbor topographic connections within the ipsilateral projection. The location of RGCs along the dorsal–ventral retinal axis dictate the location of their TZs along the ventromedial–dorsolateral axis in the dLGN, and the location of ganglion cell bodies in the nasal–temporal retinal axis determine their projections along the ventrolateral–dorsomedial axis (Fig. 3a–3h; Feldheim et al., 1998; Grubb et al., 2003). *Phr1* retinal mutants retain a topographically

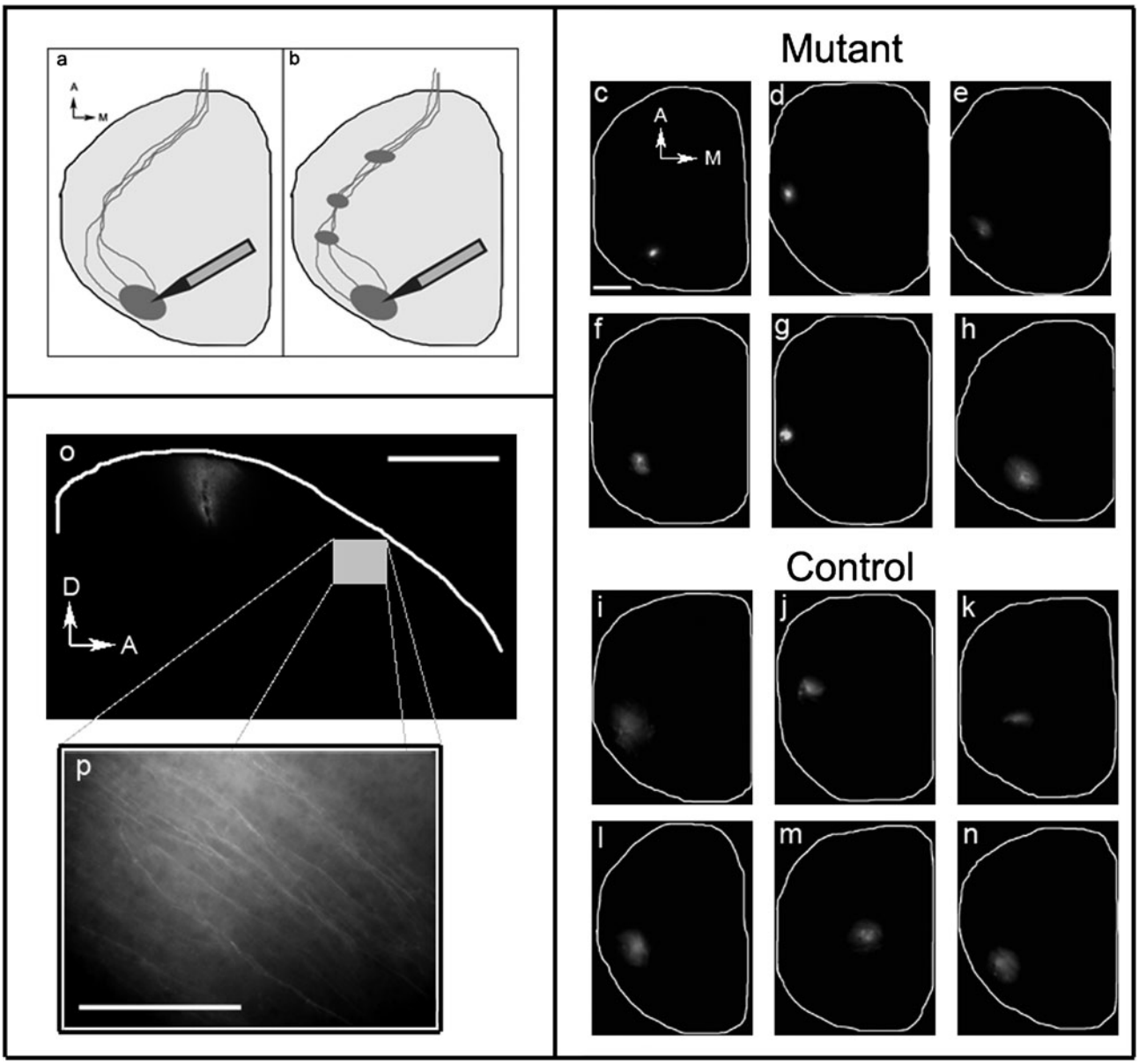

Fig. 2. Absence of ectopic terminal zones (TZs) in controls and *Phr1* mutants following DiI retrograde labeling in the posterial–lateral region in the superior colliculus (SC). Simplified diagram showing the DiI retrograde labeling (a) where anteriorly shifted TZs might result from interstitial branching (b). None of the controls or the mutant animals exhibit additional termination zone (c–n). A sagittal section of the SC shows that the DiI injection spans the entire depth of the nucleus (o). 20× magnification of the most anterior edge demonstrates that sufficient time was allowed for DiI to travel the entired span of the SC from the posterior injection site (p). Total $n = 12$, $n = 6$ for control and $n = 6$ for mutant. Scale bar = 400 μm; a, anterior; p, posterior; m, medial; d, dorsal; v, ventral.

appropriate map with only minor morphological aberrations compared to controls. Mutant ND RGC TZs were confined to the area lining the most lateral aspect of the nucleus, as in controls, although they were extended diffusely along the dorsal–ventral axis (Fig. 3a′–3d′). In contrast, injections in the TV retinal quadrant, which include both contralaterally and ipsilaterally projecting RGCs, lead to normally localized TZs in the medial aspect of the nucleus. Surprisingly, no ipsilaterally projecting axons were observed to be grossly mislocated in any of our focal dye labeling experiments despite that the ipsilateral projection, which originates in the TV quadrant, was previously shown to be mislocalized in the dLGN by bulk labeling of RGCs (Culican et al., 2009). We did not detect any contralaterally projecting axons after TV injections. This may reflect the fact that all our injections were applied at the corneal limbus, in the most peripheral aspect of the retina, where ipsilaterally projecting RGCs are more abundant. Although *Phr1* retinal mutants had a roughly normal topographical map in the dLGN, as evidenced by fairly appropriate location of TZs, we did observe more diffuse terminations in labeling from all quadrants (Fig. 3e′–3h′). Despite the similarity of this finding in both the dLGN and the SC, the disruptions found in the retinogeniculate map are more subtle than those found in the retinocollicular map, particularly regarding RGCs of the ND quadrant.

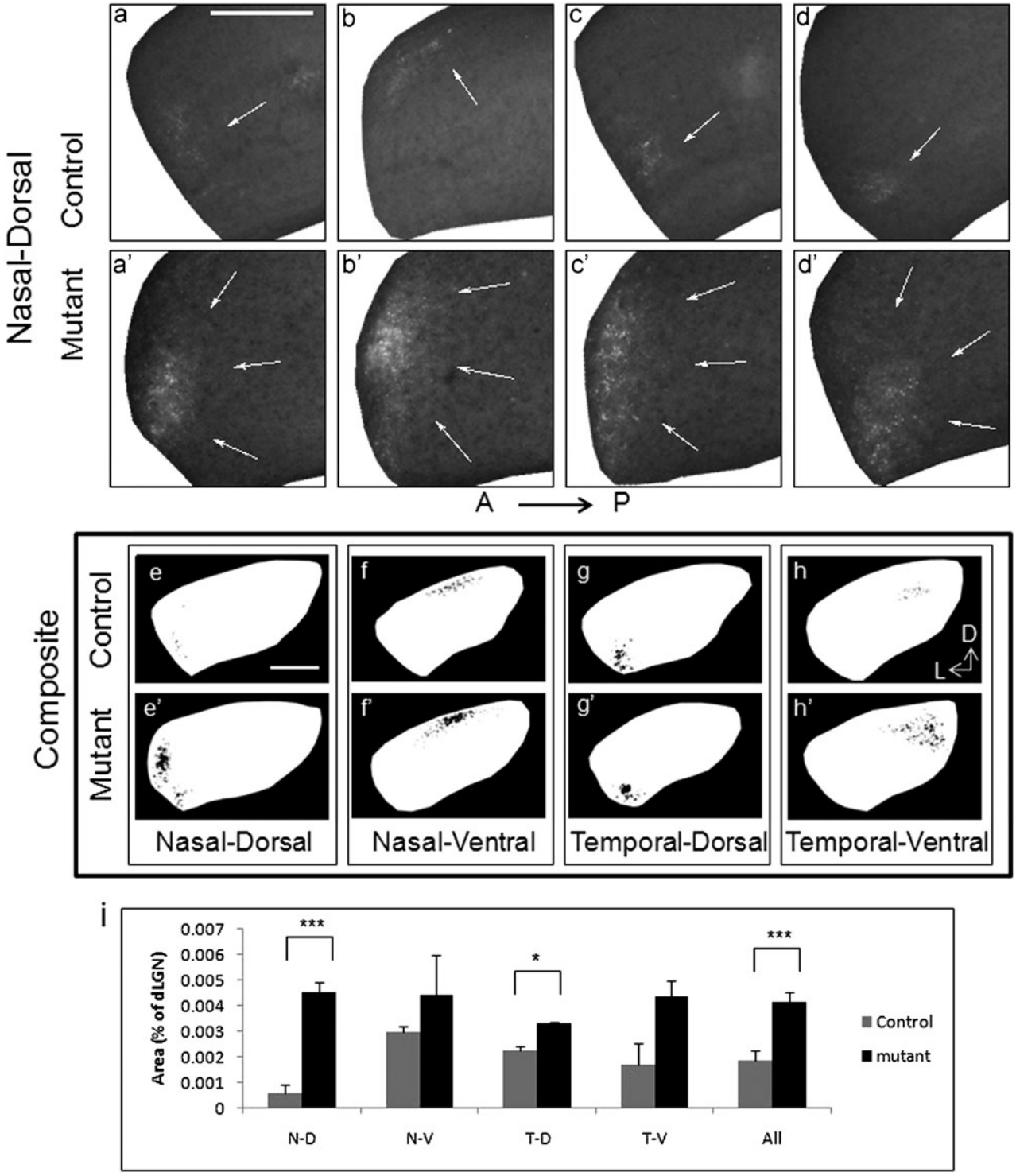

Fig. 3. Diffuse terminal zones (TZs) in dorsal lateral geniculate nucleus (dLGN) of the *Phr1* mutant. TZs are identified in coronal sections of the dLGN from anterior to posterior following DiI injection in the nasal–dorsal (ND) quadrant of the retina in control (a–d) and *Phr1* mutant (a′–d′) mice. Enlarged TZs are observed in each anterior to posterior coronal section of the dLGN with injections in the ND retinal quadrant (a′–d′). Because a TZ spans multiple anterior to posterior sections, a composite image was created by collapsing each of four individual sections (a–d), using a threshold algorithm (see Materials and methods), onto a single representative section (e). This was done to normalize comparisons between mutants and controls for TZs from the ND (e, e′), nasal–ventral (f, f′), and temporal–dorsal (TD) (g, g′) quadrants. This analysis of the contralateral projection demonstrates that TZs in the mutant are appropriately located but more diffuse compared to control TZs (e′–g′). Similarly, ipsilaterally projecting temporal–ventral TZs are also more diffuse in mutant (h) than control (h′). The diffuse TZs in the mutants occupied a significantly larger area of the dLGN than in controls, particularly from the ND ($P < 0.0005$) and TD ($P < 0.05$) quadrants (i). Error bars represent standard error mean (S.E.M.). Total $n = 16$, $n = 2$ animals for each genotype and each quadrant injected. Scale bar = 200 μm; a, anterior; p, posterior; l, lateral; d, dorsal; n, nasal; v, ventral; t, temporal.

Discussion

The proper formation of topographic maps in the visual system requires spatial relationships between RGC cell bodies preserved by their projections to central targets. During development, both molecular guidance and activity-dependent mechanisms contribute to the establishment of these retinotopic maps, and abnormalities in either mechanism lead to aberrant retinotopy such as the mislocalization of ipsilaterally projecting RGCs seen in the dLGN of *Phr1* retinal mutants. Since disturbed targeting of the ipsilateral retinogeniculate projection in this mouse is independent of spontaneous retinal activity and monocular segregation, we sought to determine if the defect represents a more general disruption of retinofugal mapping. Indeed, our results indicate that in addition to the ipsilaterally projecting RGCs, there is disruption of input localization from the contralateral eye to both the dLGN and the SC. Furthermore, we wondered whether the mislocalized ipsilateral projection demonstrates a reorientation of the overall topographic map or also the effect of disrupted local nearest-neighbor connectivity. Our results support both mechanisms: anterograde focal injections into the ND quadrant of the retina lead to multiple separate TZs in the SC, indicative of the latter, while the occurrence of diffuse TZs from all quadrants supports the former. Given the perturbed localization of the ipsilateral projection to the dLGN, the subtle finding of a modestly more diffuse TV quadrant projection, in contrast to the severely disturbed ND connectivity, was unexpected. This finding raises the possibility that *Phr1* mediates RGC axon path finding to various central targets *via* multiple mechanisms.

The mechanism by which ectopic patches arise from RGCs originating in the ND quadrant is not known. One possible mechanism is that ectopic patches result from misplaced interstitial branching. In such a case, the primary axons of ND RGCs might terminate in the appropriate zone, preserving nearest-neighbor connectivity, but additional interstitial branches would be misguided and form multiple anteriorly shifted ectopic TZs. A similar mechanism has been demonstrated in the EphB2/EphB3 double mutant where RGC axons extend interstitial branches beyond the primary TZ location, in addition to a TZ in the correct location (Hindges et al., 2002). However, the failure to demonstrate multiple TZs in mutant and control SCs retrogradely labeled in the posterial–lateral region suggests an alternative mechanism for ectopic TZs in *Phr1* retinal mutants. Thus, the *Phr1* mutant ND phenotype may result from a topographic mapping error that disrupts nearest-neighbor connectivity. Further clarification of these possibilities will require techniques for labeling single RGC axonal arbors to assess termination zones for an individual cell in both control and *Phr1* retinal mutants.

Mutant RGCs from the ND quadrant of the retina projecting to the posterolateral SC form multiple anteriorly shifted ectopic TZs. Mapping along the anterior–posterior axis of the SC is mediated by EphA/ephrin-A signaling. Gradients of EphA and ephrin-A expression run counter to each other across the mouse retina: EphAs are highly expressed in the ventral retina, while ephrin-As are enriched in the dorsal retina (Flanagan, 2006). Previous studies (Culican et al., 2009) of the *Phr1* retinal mutant focused on abnormal localization of the ipsilateral patch in the dLGN, which reflects projections from cells originating in the TV retina, a region of high EphA expression. *Phr1* mutant retinal axons were found to respond to ephrin-A *in vitro* (Culican et al., 2009), indicating that EphA-mediated receptor signaling is intact. Given that ephrin-As are cell surface ligands anchored to the cell membrane via a Glycosylphosphatidylinositol (GPI) linkage and EphAs are receptor tyrosine kinases, this finding appeared to exclude a disruption of EphA/ephrin-A signaling in the *Phr1* retinal mutant. However, recent findings indicate that GPI-linked ephrin-As are capable of reverse signaling (Lim et al., 2008). Moreover, nasal RGCs, which express a high level of ephrin-A, erroneously map anterior to their correct termination zone in the SC when ephrin-A reverse signaling is perturbed (Hornberger et al., 1999; Lim et al., 2008). A similar anteriorly shifted phenotype is seen in the *Phr1* retinal mutant, specifically in the ND quadrant, leading us to hypothesize a possible role of ephrin-A reverse signaling independent of EphA forward signaling in the *Phr1* mutant.

The observation of enlarged and diffuse TZs in retinofugal projections of the *Phr1* mutant is curious. This phenotype is typically seen in animals with disrupted retinal wave activity. Mice lacking the $\beta 2$ subunit of the Nicotinic Acetylcholine Receptor ($\beta 2^{-/-}$) display enlarged, dispersed, and patchy TZs in the dLGN and SC resulting from lack of axonal refinement (Grubb et al., 2003; Chandrasekaran et al., 2005). There is evidence to suggest that in addition to activity, activity-independent molecular cues regulate this process. EphBs and ephrin-Bs, for example, play an important role in axon terminal refinement through synaptogenesis, directional branch extension, and arborization (Hindges et al., 2002; McLaughlin et al., 2003). It is unlikely that *Phr1* acts *via* an EphB/ephrin-B–mediated process because their role in topographic mapping has been demonstrated to mediate medial–lateral positioning and we saw no significant disruption in that anatomic axis. However, because the *Phr1* retinal mutant demonstrates normal spontaneous retinal wave activity (Culican et al., 2009), we propose that *Phr1*, like the EphBs/ephrin-Bs, is an activity-independent regulator of TZ refinement. The mechanism by which *Phr1* acts independently of retinal activity to direct proper retinotopic placement as well as the refinement of RCG axons within their targets is undefined. Additional studies of the molecular pathways that determine *Phr1* function will help elucidate its role in controlling these cellular processes.

Acknowledgments

We are very grateful to David Simon for experimental advice and assistance. We also recognize Joseph Mertz and Oloruntoyin Falola for technical support. This work was supported by the Horncrest Foundation, the NEI (K12 EY016336), and by a Research to Prevent Blindness, Inc. Unrestricted grant, and NIH Vision Core grant (P30 EY 02687) awards to the Department of Ophthalmology and Visual Sciences at Washington University.

References

Bloom, A.J., Miller, B.R., Sanes, J.R. & DiAntonio, A. (2007). The requirement for *Phr1* in CNS axon tract formation reveals the corticostriatal boundary as a choice point for cortical axons. *Genes & Development* **21**, 2593–2606.

Burgess, R.W., Peterson, K.A., Johnson, M.J., Roix, J.J., Welsh, I.C. & O'Brien, T.P. (2004). Evidence for a conserved function in synapse formation reveals *Phr1* as a candidate gene for respiratory failure in newborn mice. *Molecular & Cellular Biology* **24**, 1096–1105.

Chandrasekaran, A.R., Plas, D.T., Gonzalez, E. & Crair, M.C. (2005). Evidence for an instructive role of retinal activity in retinotopic map refinement in the superior colliculus of the mouse. *The Journal of Neuroscience* **25**, 6929–6938.

Culican, S.M., Bloom, A.J., Weiner, J.A. & DiAntionio, A. (2009). *Phr1* regulates retinogeniculate targeting independent of activity and ephrin-A signaling. *Molecular & Cellular Neurosciences* **41**, 304–312.

DiAntonio, A., Haghighi, A.P., Portman, S.L., Lee, J.D., Amaranto, A. M. & Goodman, C.S. (2001) Ubiquitination-dependent mechanisms regulate synaptic growth and function. *Nature* **412**, 449–452.

D'Souza, J., Hendricks, M., Le Guyader, S., Subburaju, S., Grunewald, B., Scholich, K. & Jesuthasan, S. (2005). Formation of the retinotectal projection requires Esrom, an ortholog of PAM (protein associated with Myc). *Development* **132**, 247–256.

Feldheim, D.A., Kim, Y.I., Bergemann, A.D., Frisen, J., Barbacid, M. & Flanagan, J.G. (2000). Genetic analysis of ephrin-a2 and ephrin-a5 shows their requirement in multiple aspects of retinocollicular mapping. *Neuron* **25**, 563–574.

Feldheim, D.A., Vanderhaeghen, P., Hansen, M.J., Frisen, J., Lu, Q., Barbacid, M. & Flanagan, J.G. (1998). Topographic guidance labels in a sensory projection to the forebrain. *Neuron* **21**, 1303–1313.

Flanagan, J.G. (2006). Neural map specification by gradients. *Current Opinion in Neurobiology* **16**, 59–66.

Grubb, M.S., Rossi, F.M., Changeux, J.P. & Thompson, I.D. (2003). Abnormal functional organization in the dorsal lateral geniculate nucleus of mice lacking the beta 2 subunit of the nicotinic acetylcholine receptor. *Neuron* **40**, 1161–1172.

Hindges, R., McLaughlin, T., Genoud, N., Henkemeyer, M. & O'Leary, D.D. (2002). EphB forward signaling controls directional branch extension and arborization required for dorsal-ventral retinotopic mapping. *Neuron* **35**, 475–487.

Hornberger, M.R., Dütting, D., Ciossek, T., Yamada, T., Handwerker, C., Lang, S., Weth, F., Huf, J., Webel, R., Logan, C., Tanaka, H. & Drescher, U. (1999). Modulation of EphA receptor function by coexpressed ephrinA ligands on retinal ganglion cell axons. *Neuron* **22**, 731–742.

Lewcock, J.W., Genoud, N., Lettieri, K. & Pfaff, A.L. (2007). The ubiquitin ligase *Phr1* regulates axon outgrowth through modulation of microtubule dynamics. *Neuron* **56**, 604–620.

Lim, Y., McLaughlin, T., Sung, T., Santiago, A., Lee, K. & O'Leary, D. M. (2008). p75(NTR) mediates ephrin-A reverse signaling required for axon repulsion and mapping. *Neuron* **59**, 746–758.

Luo, L. & Flanagan, J.G. (2007). Development of continuous and discrete neural maps. *Neuron* **56**, 284–300.

McLaughlin, T., Hindges, R., Yates, P.A. & O'leary, D.D. (2003). Bifunctional action of ephrin-B1 as a repellent and attractant to control bidirectional branch extension in dorsal-ventral retinotopic mapping. *Development* **130**, 2407–2418.

McLaughlin, T. & O'Leary, D.D. (2005). Molecular gradients and development of retinotopic maps. *Annual Review of Neuroscience* **28**, 327–355.

Pfeiffenberger, C., Yamada, J. & Feldheim, D.A. (2006). Ephrin-As and patterned retinal activity act together in the development of topographic Maps in the primary visual system. *The Journal of Neuroscience* **26**, 12873–12884.

Reese, B.E. (2010). Development of the retina and optic pathway. *Vision Research* doi: 10.1016/j.visres.2010.07.010.

Schaefer, A.M., Hadwiger, G.D. & Nonet, M.L. (2000). *rpm-1*, a conserved neuronal gene that regulates targeting and synaptogenesis in C. elegans. *Neuron* **26**, 345–356.

Simon, D.K. & O'Leary, D.D. (1991). Relationship of retinotopic ordering of axons in the optic pathway to the formation of visual maps in central targets. *The Journal of Comparative Neurology* **307**, 393–404.

Sperry, R.W. (1963). Chemoaffinity in the orderly growth of nerve fiber patterns and connections. *Proceedings of the National Academy of Sciences of the United States of America* **50**, 703–710.

Torborg, C.L. & Feller, M.B. (2005). Spontaneous pattern retinal activity and the refinement of retinal projection. *The Journal of Neuroscience* **76**, 213–235.

Wan, H.I., DiAntonio, A., Fetter, R.D., Bergstrom, K., Strauss, R. & Goodman, C.S. (2000). Highwire regulates synaptic growth in Drosophila. *Neuron* **26**, 313–329.

Yang, Z., Ding, K., Pan, L., Deng, M. & Gan, L. (2003). Math5 determines the competence state of retinal ganglion cell progenitors. *Developmental Biology* **264**, 240–254.

Zhen, M., Huang, X., Bamber, B. & Jin, Y. (2000). Regulation of presynaptic terminal organization by *C. elegans* RPM-1, a putative guanine nucleotide exchanger with a RING-H2 finger domain. *Neuron* **26**, 331–334.

Supplementary Data

Supplemental material can be viewed in this issue of *Visual Neuroscience* by visiting journals.cambridge.org/VNS

Fig. S1. Qualitative presentation of area (in percentage) of terminal zones (TZs) in the dorsal lateral geniculate nucleus (dLGN): The dLGN was outlined in epifluorescence images manually based on gross anatomical morphology. Background was determined from measurement of a nonlabeled area of the dLGN and was digitally subtracted from the entire image. A threshold was set at 20% of the maximum signal intensity, and the image converted to a binary image. Four binary images were then aligned by dividing the nucleus evenly along the dorsal–ventral and medial–lateral axis and aligning the images at the intersection of these axes. The threshold pixels were then collapsed into a single composite image (**e**). This process was repeated for each of the quadrants injected and for each genotype (b→f, b′→f′, c→g, c′→g′, d→h, d′→h′).